Chapter

Very Low Voltage and High Efficiency Motorisation for Electric Vehicles

Daniel Matt and Nadhem Boubaker

Abstract

This chapter details the design of a new innovative solid bar winding for electrical machines (either motors or generators) dedicated to the electric propulsion. The goal of this new winding technique is to enhance the performance by better utilizing the stator slot and increasing the copper fill factor to higher than 75%, and also to reduce the inactive copper at the end-windings. Accordingly, many advantages arise from the application of this solid bar winding: higher torque-to-weight ratio, better thermal behavior, lower rotor losses, higher efficiency, higher reliability and lower cogging torque. However, the solid bar has its inherent constraints, which should be considered with care when designing an electric motor: the AC copper losses and the manufacturing process. The suggested winding technique aims at addressing these challenges.

Keywords: solid bar winding, permanent magnet synchronous machine, high performance electric motor, high power-to-weight ratio, electric propulsion, AC copper loss, low voltage winding, high slot fill factor

1. Introduction

The need for a higher competitive electrical machines, mainly in terms of power density and efficiency, is increasing especially in embedded applications (aerospace, Vertical Take-Off and Landing, Electric Vehicle, etc.); these performances are a key differentiator between competitors. As a rule of thumb, nowadays, a good power-to-weight ratio of PM electric motors is around 3 kW/kg (EMAG + mechanical packaging) [1]. Nevertheless, higher values have been proclaimed by many companies and star-ups, but for experimental prototypes where the maturity of the product is still questionable. The definition of the power to weight ratio is still versatile and controversial because, on one hand, the estimation of the total motor weight relies on many parts where some of them are not always considered in the calculation: EMAG, mechanics, coolant weight (in some cases is shared with the system), cables, power electronic, etc., on the other hand, the flexible definition of the output power (continuous or transient).

The opportunities for achieving a big improvement against the state of the art are very limited and challenging due to the very small degree of freedom.

The following expression provides the basic relationship of the sizing electromagnetic power of electric motors (rotational movement). This expression highlight some, but not all, obvious paths to follow in order to improve the performance.

$$P = C\, k_w \lambda_e\, B\, D^2 L_s\, \Omega \tag{1}$$

Where, C: constant coefficient, k_w: winding factor, λ_e: electric loading (number of ampere-conductors per meter around the bore of the stator), B: magnetic loading (magnetic flux-density in the airgap), D: rotor diameter, L_s: stator corepack length (active length), and Ω: rotation speed.

These are the main routes to enhance the performance of the electrical machines:

- The ferromagnetic materials: there is no noticeable progress since the last 30 years on the electrical steels. The Iron Cobalt alloy (FeCo) is still the best electrical steel point of highest saturation level around 2.4 T and lowest coreloss (at a given lamination thickness and heat treatment), however is much more expensive and require a specific manufacturing process (specific annealing etc.) in comparison with other more conventional electrical steels like the Iron-Silicon alloy (FeSi) [1].

- The permanent magnet grade: the catalog of the permanent magnet suppliers has been extended in the last few years, even though there is no noticeable since many years. High-grade magnets work well at development level (prototype), but they show some serious limitations when it comes to use them in a harsh environment (NdFeB are not suitable for high temperature > 200°C), or to consider the industrialization (high volume production/cost).

- The thermal management: cooling is a key subject nowadays to push the performance of electric motors beyond certain limits. Some novel cooling technologies are very promising but not fully mature yet, such as: hollow conductor (technique so far reserved for high power machines > MW), flooded slot cooling, ...

For a given specification, the selection of an efficient cooling technique can be very challenging because it can compromise the overall performance of the system (optimisation issue) by adding cost, complexity, and weight, and compromising the reliability as well, which can be prohibitive in some embedded applications.

The bar winding presented in this chapter permits to improve the heat exchange in both the slots and the end-windings [1–3].

- The rotational speed: this has been always a research topic of interest. Very high speed motors have their own limitations and constraints, mainly mechanical (rotor sleeving, integrity of the structure, ...).

  Many applications require a rotational speed of few 1000 rpm with a minimum stage of reduction between the electric motor and the driven load (typically driven propeller of electric VTOL), which prohibit the use of very high speed motors.

- The fundamental frequency: this is largely exploited nowadays; high fundamental frequency reduce the dimensions and the mass of electrical machines by making the stator back iron and the rotor yoke very thin (few millimeters). High fundamental frequency usually leads to a high pole count paired with a concentrated winding around the tooth (q < 1) which offer a very compact motor due to the short end-windings [4].

A thin stator back iron will noticeably reduce the thermal resistance between the copper and the external cooling sources, especially for forced air-cooled motors via the housing fins.

Furthermore, halbach arrangement is suitable for this type of motors and help getting rid of the rotor yoke, by, for example, gluing the magnets on a non-magnetic wheel such as aluminum or composite material in order to further reduce the weight.

- The electric loading: this is an avenue for improvement, especially through the use of superconducting materials. There definitely has been a lot of progress, but the materials with low critical temperature have not given the expected results so far and the associated cooling devices prohibits any on-board use.

We suggest in this chapter to focus on a different approach to increase the performance of the electric motors by using a new winding technique with solid bars in order to improve the copper fill factor in the slot [1–3]. The fill factor of a conventional electrical machine with random round wire is always less than 45% (CSA pure copper/CSA naked slot). The use of a solid conductor allows reaching higher fill factor at least 75% and consequently enhances the performance of electric motors.

2. Advantages of the solid bar winding

Despite these attractive advantages, the use of solid bar in the armature winding of synchronous machines has been reserved to very limited applications such as MW turbo generators and the aircraft 3-stage generators (APUG, VFG, IDG). Such a winding type becomes more and more common while being introduced in the electric and hybrid electric vehicle for a medium power ranging from 40 kW to 200 kW, it is called hairpin winding. A winding of this ilk is ideal to provide the needed performance when the traction motor of the vehicle required to develop high torque at low speed or during accelerations.

The winding covered in this chapter is different from the hairpin winding and has been used for many applications: electric vehicle, small sport car, utility vehicles, full electric boat, ...

2.1 Enhanced slot fill factor greater than 80%, so better performance and better thermal behavior at both the slots and the end-windings

The performance of any electrical machine is intimately linked to the slot fill factor. There few definition of slot fill factor, here we consider the ratio of total pure copper in one slot per total slot area.

In a conventional overlapping winding with round wire, the copper fill factor is always mediocre and it is very complicated to exploit beyond 45% of the slot area (non-segmented stator), so almost half of the slot volume is inactive and occupied by the air and the different insulation materials (cf. **Figure 1**).

As regards the solid conductor winding we propose here, the slot fill factor is typically higher than 75%. Indeed, the bar is housed in a rectangular slot slightly larger than the bar to allow the slot insulation (slot liner). The slot dimensions are equal to: $w_{slot} = w_{bar} + \delta_{sl}$ and $h_{slot} = h_{bar} + \delta_{sl}$, where δ_{sl} is the gap between the slot wall and the solid conductor intended to receive the slot liner. δ_{sl} typically lies between 0.3 mm and 0.5 mm ($V < 1$ kV and $P < 300$ kW).

Improving the slot fill factor with solid bar will introduce these benefits:

- At a given electric loading and given DC copper loss: when the copper fill factor is improved, the height/size of the slot can be reduced in the same

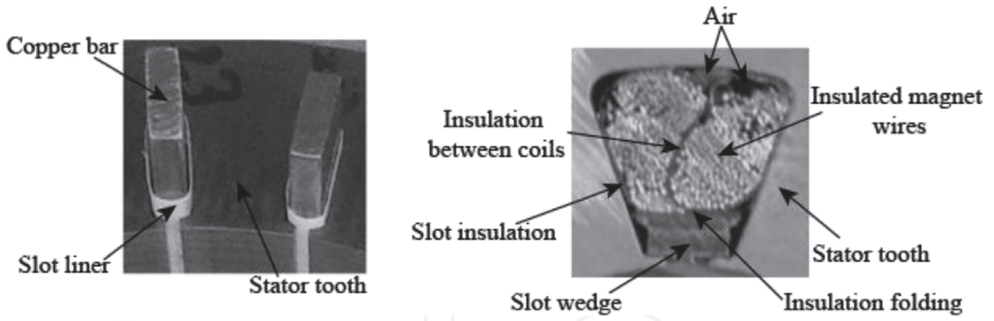

Figure 1.
Illustration of the slot fill factor with round wire and with the solid bar proposed in this paper.

	20% fill factor	40% fill factor (baseline)	80% fill factor	90% fill factor
CSA copper in the slot [PU]	0.5	**1**	2	2.25
Total current in the slot [PU]	0.7071	**1**	1.4142	1.5
Current density J [PU]	1.4142	**1**	0.7071	0.6667
Electric loading λ [PU]	0.7071	**1**	1.4142	1.5000
Copper loss [PU]	1	**1**	1	1
Copper mass [PU]	0.5	**1**	2	2.25
Torque [PU]	0.7071	**1**	1.4142	1.5
Total EMAG weight [PU]	0.9	**1**	1.2	1.25
Copper weight / Total EMAG weight ratio [PU]	0.111	**0.2**	0.333	0.360
Torque-to-weight ratio [PU]	0.7857	**1**	1.18	1.20

Table 1.
Motor performance (per unit calculation) versus slot fill factor, at a given slot area and a given DC copper losses.

proportion. A shorter slot leads to a smaller and lighter motor by reducing its outer diameter; or, at a given motor outer diameter (envelope), the stator inner diameter can be increased and, hence, the output torque.

- At a given slot area and a given DC copper losses: a better copper fill factor will permit to increase the torque-to weight ratio of the motor while keeping the same efficiency. For example, increasing the fill factor from 40% with round wire to 80% with solid bars (both values are practical) will permit to multiply the current in the slot by $\sqrt{2}$ and consequently getting +18% torque-to-weight ratio assuming that the copper is around 20% of the total EMAG weight. A per unit calculation is shown in the **Table 1** in order to give an overview of the motor performance for a copper fill factor lying between 20% and 90%, where the baseline case is 40% fill factor (well known value for a standard manufacturing).

In practice, it might be possible to increase the copper loss density in the solid bar winding because the thermal exchanges between the copper and the stator corepack and between the end-windings and the housing are improved (cf. **Figure 1**).

Enhancing the thermal management with solid bar will permit to homogenize the copper temperature and suppress the hotspots, which makes the winding insulation more reliable.

2.2 Less bulky, lighter, and better controlled end-winding, so higher power density and efficiency

The end-windings are always representing an Achilles heel for electric actuators. Indeed, they dissipate the energy without contributing to the creation of useful power. Hotspots usually occur in this part of the winding. The prediction of the volume of the end-windings is difficult, because the geometry is complex and dependent on several poorly controlled factors, such as the winding topology, the tact of the engineer or the machine carrying out the winding,...

In practice, to approximately take into account the loss in the end-windings with round wire in the calculation of the efficiency, the designers multiply the Joule loss dissipated in the slots by an add-on factor generally lying between 1.3 and 2 (distributed winding). It is not unusual to encounter a short electrical machine with end-winding factor of 2; it means that the half-turn axial length is equal to the double of the stator active length (stack length) and therefore the loss in the end-windings are equal to the loss in the active copper located in the slots.

For the bar winding that we propose here, the end-windings volume can be precisely estimated via the relation (13) or (14). Accordingly, the end-windings Joule loss can be accurately predicted as well as the global efficiency of the machine.

Furthermore, we gain in space (shorter machine) and weight and thus better power density and efficiency (**Figure 2**).

2.3 Less constraining slot opening, so improved cogging torque and rotor losses

Despite the fact that some performance of the electrical machine are closely linked to the slotting effect, the slot opening width is not really an optimization parameter in the case of a conventional winding, because it is imposed by the winder to facilitate the insertion of the coils into the slots.

The performance related to the slot opening are:

- Rated torque: the modulation of the flux density caused by the slotting effect impairs the fundamental of the airgap flux density (larger effective airgap) and consequently affects the produced torque.

- Cogging torque: the smoother the stator bore the lower the slotting effect and the cogging torque. This improves the acoustic and vibration behavior of the machine.

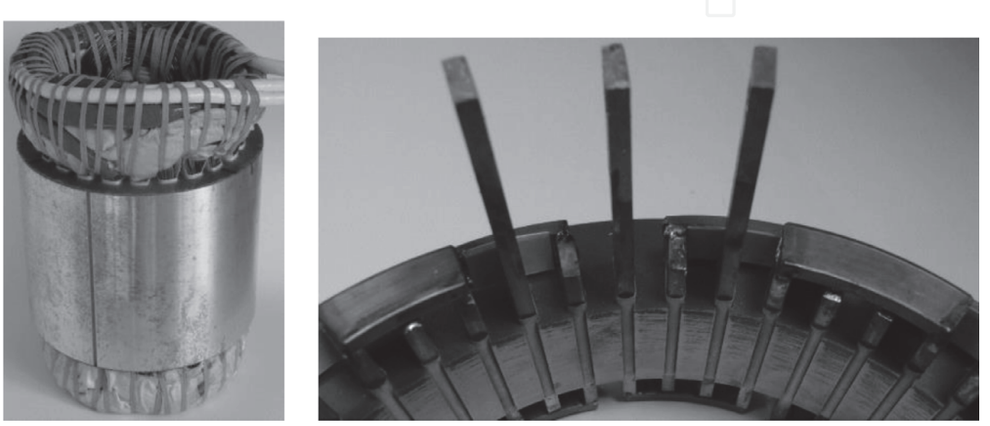

Figure 2.
End-windings of round wire winding (left) - End-windings of solid bar winding (right).

- Rotor eddy-current losses in the magnets, in the conducting retaining sleeve, and in the solid iron rotor: a low slot opening width will significantly mitigate the airgap reluctance modulation seen by the rotor and consequently less induced loss and better efficiency.

- The windage loss: is proportional to the roughness coefficient that depends directly on the surface state of the rotor and stator. It is minimal (∼1) for a machine with a smooth rotor and low slot opening.

In the case of bar winding, there is no particular constraint on the slot opening because the conductors are inserted by sliding into the stator, which allows to optimize it and to improve the aforementioned performance. The optimum slot opening width with the bar winding proposed in this paper is typically lying between 0.5 mm and 1 mm. It corresponds to a trade-off between a minimal slotting effect and minimal leakage flux (highest produced torque).

3. Novel solid bar winding for electrical machines

3.1 Design principle and manufacturing steps

Unlike the malleable round wire winding, the main complexity of a bar distributed winding is the connection of the overlapping poles at the end-windings level. To overcome this difficulty we have designed a relatively simple system to enable the end-windings connection by means of bent bars alternating overhead and frontally as shown in **Figure 3**, we called them "bow bar" and "crook bar". The latter are brazed to the bars located in the slots and they have the same cross section (but could be different shape). According to the **Figure 3**, we can distinguish three different lengths of the bars located in the slots: short bar (bow/bow connection), medium bar (bow/crook), and long bar (crook/crook).

The assembly of the proposed bar winding can be broken down into four main steps:

- Cutting of the bars under the different lengths and then the bending of the end-windings connection bars.

- Insulating the stator core with a slot liner made from sheets of material such as: Nomex, Kapton, Dacron-Mylar-Dacron, ...

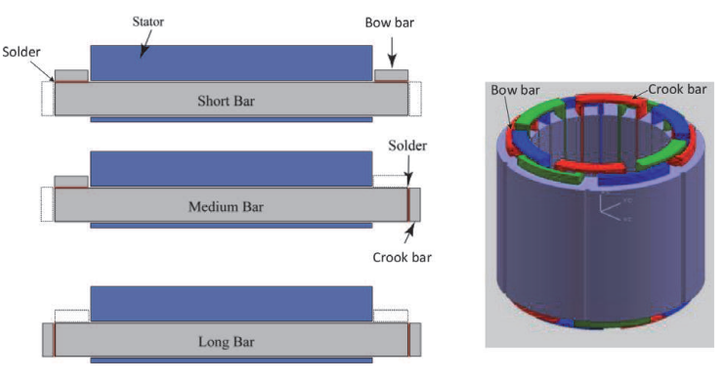

Figure 3.
Illustration of the three different end-winding connections, from the top to the bottom: Bow/bow connection, bow/crook connection, and crook/crook connection.

- Insertion of the bars into the slots and joining them to the end-windings bars. Depends on the application (temperature and vibration level), we propose two approaches to connect the end-windings, the first method is based on the soldering only, whereas the second one is using both soldering and screws into threaded holes drilled in the copper.

- Finally, the encapsulation or impregnation of the winding to reinforce the electrical insulation, increase the mechanical strength of the bars, and improve the heat exchange (especially at the end-windings).

3.2 Analytical relationships governing the proposed winding technique

In this part, we propose some practical and generalized analytical relationships allowing a quick determination of the dimensional characteristics of the proposed winding.

We consider the case of three-phase distributed winding, with one slot per pole and per phase (q = 1), and star connection.

The proposed relationships depend on whether the number of pole pairs, p, is even or odd. To facilitate the determination of these relationships, we consider the developed winding layout shown in **Figure 4(a)** (p is even: 4p, 24 s) and **Figure 4(b)** (p is odd: 5p, 30s).

According to the **Figure 4**, we can clearly note the different lengths of bars stated earlier in the previous section: short bar (bow/bow), medium bar

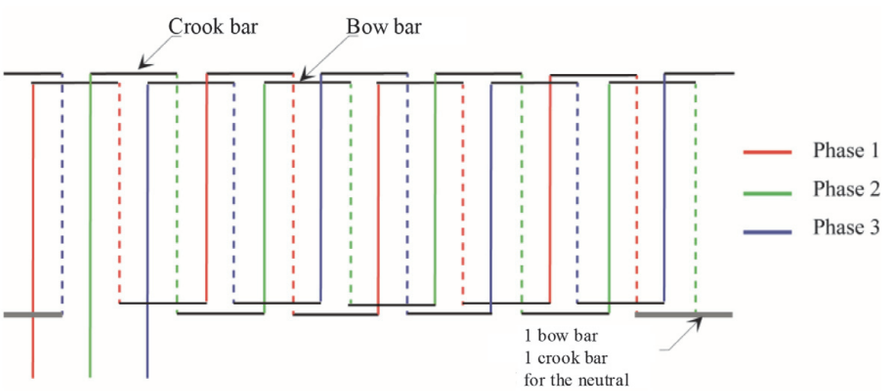

(a)

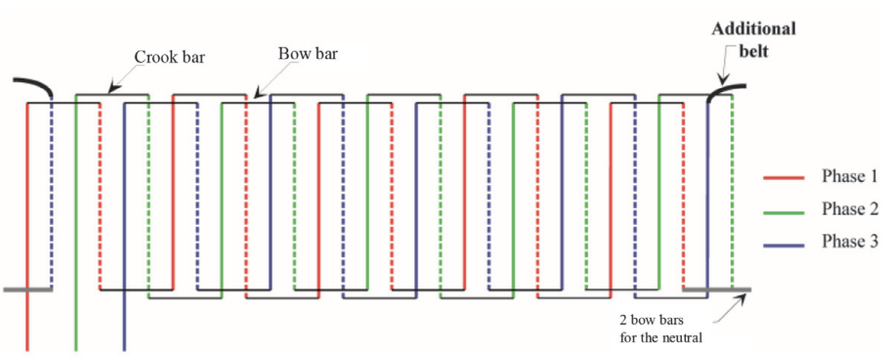

(b)

Figure 4.
Developed winding layout, for two different cases: 4p/24 s and 5p/30s. (a) p = 4. (b) p = 5.

(bow/crook), and long bar (crook/crook). We also note that if p is even the connection of the neutral is ensured by an "bow bar" and "crook bar", whereas if p is odd the connection of the neutral is performed with two "bow bars".

3.2.1 Number of the different bars

If p is even, the number of short bars, n_{sb}, the number of medium bars, n_{mb}, the number of long bars, n_{lb}, the number of bow connection bars (including neutral), n_{bb}, and the number of crook connection bars (including neutral), n_{cb}, are given by the following relationships:

$$n_{\mathrm{sb}} = \frac{\mathrm{N_{slot}} - 8}{4} + 1 \tag{2}$$

$$n_{\mathrm{mb}} = 2\frac{\mathrm{N_{slot}} - 8}{4} + 2 = 2\,n_{\mathrm{sb}} \tag{3}$$

$$n_{\mathrm{lb}} = \frac{\mathrm{N_{slot}} - 8}{4} + 2 = n_{\mathrm{sb}} + 1 \tag{4}$$

$$n_{\mathrm{bb}} = \frac{2\mathrm{N_{slot}} - 8}{4} + 2 = n_{\mathrm{cb}} + 1 \tag{5}$$

Otherwise, if p is odd:

$$n_{\mathrm{sb}} = \frac{\mathrm{N_{slot}} - 6}{4} + 1 \tag{6}$$

$$n_{\mathrm{mb}} = 2\frac{\mathrm{N_{slot}} - 6}{4} + 2 = 2\,n_{\mathrm{sb}} \tag{7}$$

$$n_{\mathrm{lb}} = \frac{\mathrm{N_{slot}} - 6}{4} = n_{\mathrm{sb}} - 1 \tag{8}$$

$$n_{\mathrm{bb}} = \frac{2\mathrm{N_{slot}} - 8}{4} + 2 = n_{\mathrm{cb}} + 2 \tag{9}$$

The sum of the different bars must satisfy this relationship:

$$n_{\mathrm{sb}} + n_{\mathrm{mb}} + n_{\mathrm{lb}} = N_{\mathrm{slot}} - 3 = 6p - 3 \tag{10}$$

where N_{slot} is the stator slot number.

3.2.2 Total volume and length of the copper: end-winding ratio

One of the main advantages of the proposed bar winding, with respect to the conventional round wire winding, is that the end-winding copper volume can be accurately estimated from the machine's basic parameters (conductor height/width, slot number etc.).

All the machine's dimensions necessary to calculate the total length of the copper as well as the end-winding ratio are illustrated in the **Figure 5**.

The total volume of the winding copper, $V_{CopperTot}$, could be split into two parts: the copper located in the slots, $V_{CopperSlot}$, and the copper in the end-windings, $V_{CopperEW}$:

$$\mathrm{V_{CopperTot}} = \mathrm{V_{CopperSlot}} + \mathrm{V_{CopperEW}} \tag{11}$$

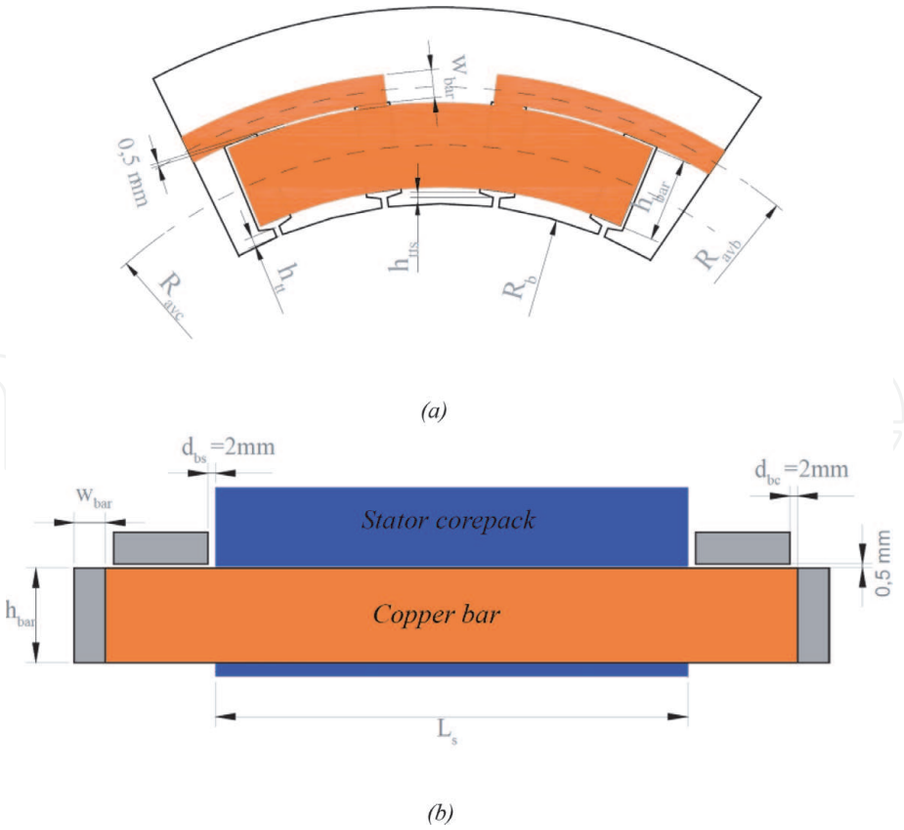

Figure 5.
Geometrical parameters of the proposed solid bar winding. (a) Front view. (b) Longitudinal section view.

The end-winding copper is the sum of the bent connection bars (bow and crook) and the part of the bars located in the slots which overhangs the stator magnetic core.

Hence, $V_{CopperSlot}$ and $V_{CopperEW}$ could be accurately estimated by means of the relations (12), (13), and (14).

$$V_{CopperSlot} = N_{slot}\, h_{bar} w_{bar} L_s \tag{12}$$

where L_s is the length of the stator core pack; h_{bar} and w_{bar} are the height and the width of the solid conductor respectively.

If p is even:

$$\begin{aligned} V_{CopperEW} = h_{bar} w_{bar} \Big[& 2\, n_{sb}(h_{bar} + d_{bs}) + n_{mb}(2\, h_{bar} + 2\, d_{bs} + d_{bc}) \\ & + 2\, n_{lb}(h_{bar} + d_{bs} + d_{bc}) + (n_{cb} - 1)\left(\frac{6\pi}{N_{slot}} R_{avc} + w_{bar}\right) \\ & + (n_{bb} - 1)\left(\frac{6\pi}{N_{slot}} R_{avb} + w_{bar}\right) + \frac{4\pi}{N_{slot}}(R_{avc} + R_{avb}) + 2\, w_{bar} \Big] \end{aligned} \tag{13}$$

Otherwise, if p is odd:

$$\begin{aligned} V_{CopperEW} = h_{bar} w_{bar} \Big[& 2\, n_{sb}(h_{bar} + d_{bs}) + n_{mb}(2\, h_{bar} + 2\, d_{bs} + d_{bc}) \\ & + 2\, n_{lb}(h_{bar} + d_{bs} + d_{bc}) + n_{cb}\left(\frac{6\pi}{N_{slot}} R_{avc} + w_{bar}\right) \\ & + (n_{bb} - 2)\left(\frac{6\pi}{N_{slot}} R_{avb} + w_{bar}\right) + \frac{8\pi}{N_{slot}} R_{avb} + w_{bar} \Big] \end{aligned} \tag{14}$$

We may express the total volume of the winding copper, $V_{CopperTot}$, as equal to the product $L_{CopperTot}\, h_{bar}\, w_{bar}$, where $L_{CopperTot}$ is the total length of the winding (3 phases) and can be inferred from the previous relations (12), (13) and expressed as:

$$\begin{aligned} L_{CopperTot} = \Big[& N_{slot} L_s + 2\, n_{sb}(h_{bar} + d_{bs}) + n_{mb}(2\, h_{bar} + 2\, d_{bs} + d_{bc}) \\ & + 2\, n_{lb}(h_{bar} + d_{bs} + d_{bc}) + (n_{cb} - 1)\left(\frac{6\pi}{N_{slot}} R_{avc} + w_{bar}\right) \\ & + (n_{bb} - 1)\left(\frac{6\pi}{N_{slot}} R_{avb} + w_{bar}\right) + \frac{4\pi}{N_{slot}}(R_{avc} + R_{avb}) + 2w_{bar} \Big] \end{aligned} \quad (15)$$

The end-winding ratio, τ_{EW}, which represents the ratio of the overhangs copper to the total winding copper, can be easily and precisely estimated via the relations (12) and (13) or (14):

$$\tau_{EW} = \frac{V_{CopperEW}}{V_{CopperTot}} = \frac{V_{CopperEW}}{V_{CopperSlot} + V_{CopperEW}} \quad (16)$$

Relation 15 gives an idea about the copper wasted in the end-winding which is inactive because it does not participate in the creation of the torque. The lower is τ_{EW} the higher are the performance of the machine in terms of power density and efficiency.

3.2.3 DC copper loss

Once the section of the conductor is known as well as the total length of the copper (cf. calculation in the previous section), the DC Joule loss can be accurately estimated from the following relation:

$$\begin{aligned} P_{ohmic} &= \rho_{20C}\left(1 + 0.004\,(T_{op} - 20)\right) \frac{L_{CopperTot}}{h_{bar} w_{bar}} I_{rms}{}^2 \\ &= \rho_{20C}\left(\frac{234.5 + T_{op}}{235.5 + 20}\right) \frac{L_{CopperTot}}{h_{bar} w_{bar}} I_{rms}{}^2 \end{aligned} \quad (17)$$

where ρ_{20C} is the copper electrical resistivity at 20°C and T_{op} is the copper operating temperature.

The solid copper conductor is always prone to supplementary loss called AC copper loss. This topic is treated in the next section.

4. AC copper loss in solid conductor winding

A solid conductor is very favorable to additional losses due to the eddy-currents and circulating currents. Special attention must be paid to the bar design according to the frequency, otherwise the AC electrical resistance could increase tremendously. The cross-section area of the conductor is then restricted in the solid bar winding, which is a drawback. This problem does not arise for round wire winding where the use of stranded, insulated, and twisted wires (Litz wire) enable to overcome this limitation.

Three different phenomena could contribute to increase the loss in a solid conductor of electrical machines: the skin effect, the slot leakage flux, and the rotating field. A three-dimensional illustration of these effects is given in the **Figure 6**.

4.1 Skin effect in a solid conductor

It is the well-known effect that tends to concentrate the current at the periphery of the conductor, this in an increasingly way as the frequency increases. The skin effect is due to opposing eddy-currents induced by the varying magnetic field, B_{in} in the **Figure 6**, resulting from the alternating current.

The **Figure 7** illustrates the skin effect in a solid copper bar with a cross-sectional area of 4x12 mm^2 and carrying an alternative current at 550 Hz.

The resistance factor, K_{skin}, which is the ratio of the AC effective resistance to the DC ohmic resistance, related to the skin effect in a solid rectangular conductor could be predicted from the Levasseur's relation [5]:

$$K_{skin} = \frac{R_{AC}}{R_{DC}} = \sqrt[6]{0.178 + \left(\frac{h_{bar} w_{bar}}{2(h_{bar} + w_{bar})} \sqrt{\sigma \mu \pi f}\right)^6} + 0.25 \qquad (18)$$

where $\mu = \mu_0 \mu_r$: the magnetic permeability, σ: the electrical conductivity, f: the frequency of the current.

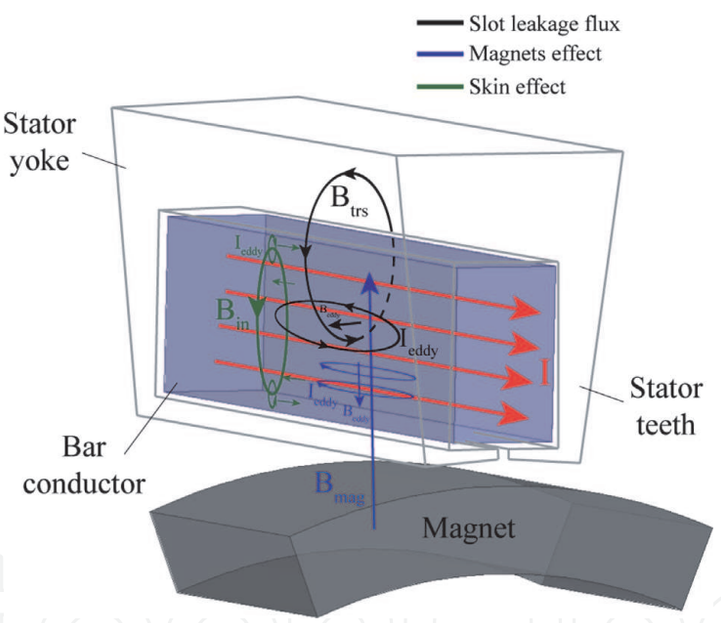

Figure 6.
3D representation of the magnetic fields and their associated eddy-currents in a solid bar winding.

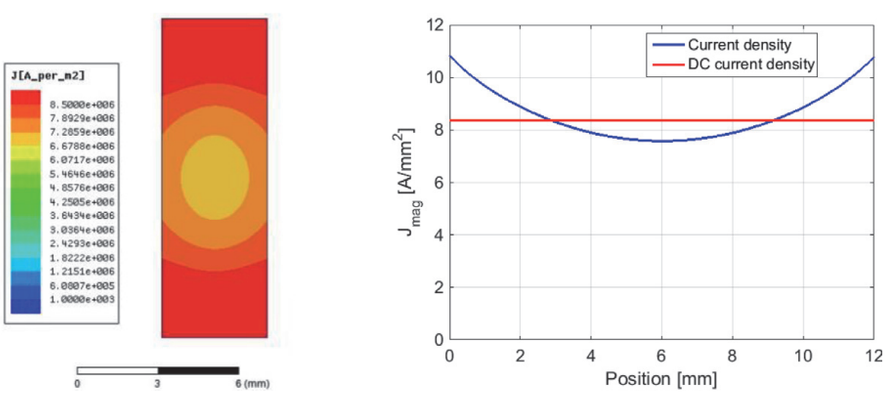

Figure 7.
Skin effect in a rectangular solid bar.

For a better use of the copper area, the goal is always to obtain K_{skin} close to the unit.

The pure skin effect only concerns the end-windings, which is the part of the copper in the air.

For example, at f = 1000 Hz, h_{bar} = 6 mm and w_{bar} = 4 mm, the resistance factor K_{skin} is circa 1.05. For the considered frequencies, the conventional skin effect is negligible compared to the effect of the current displacement occurring inside the slots, cf. next section.

4.2 Effect of the cross-slot leakage flux: critic height of the solid bar

4.2.1 Effect of the cross-slot leakage - field effect

The slot leakage flux could create an extra copper loss in solid conductors surrounded by a magnetic material. This is an old phenomenon that was treated on large alternators and frequently called Field effect.

Indeed, the alternating leakage field due to the armature current, represented by B_{trs} in **Figure 6**, tends to close through the stator slot and create eddy-currents that oppose the main current at the bottom of the slot and are superposed to it near to the slot opening. This induces an increased current density in the conductor cross-sectional area close to the bore of the stator. Hence, the unequal current distribution results in increased effective resistance and consequently higher copper loss.

The **Figure 8** shows 2D and 3D illustrations of the irregular current distribution in a solid copper bar surrounded by a magnetic material, with a cross-sectional area of 4x12 mm^2 and carrying an alternative current at 550 Hz.

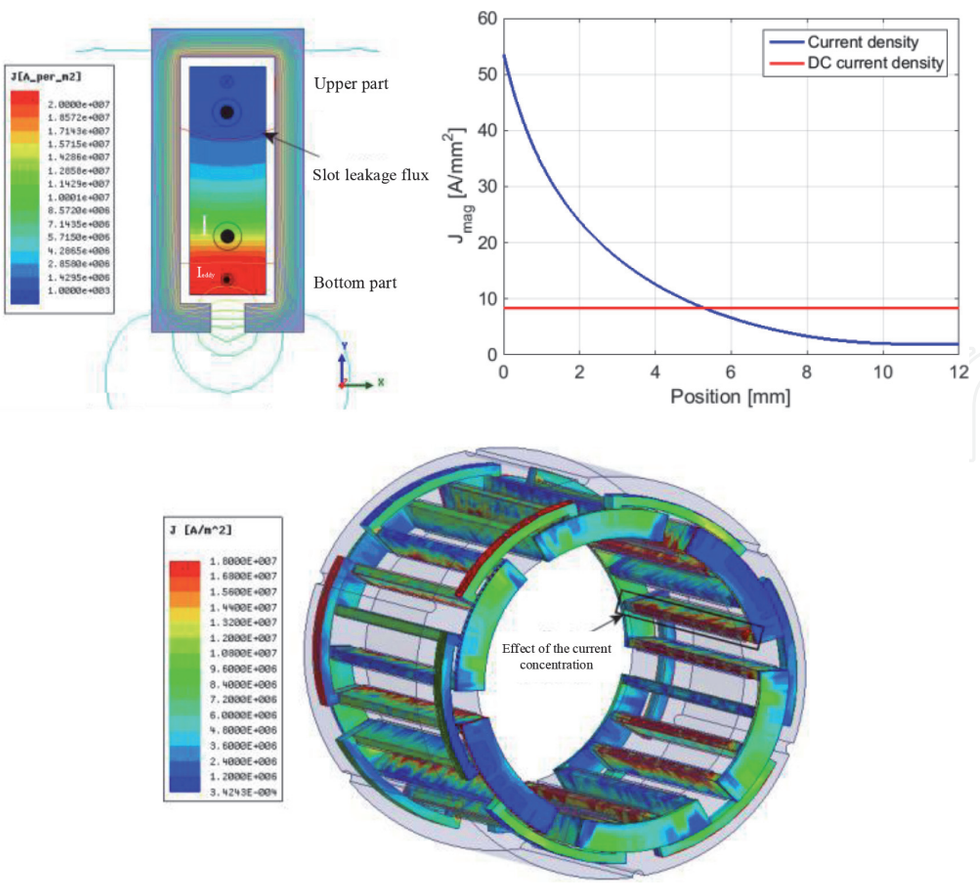

Figure 8.
Non-uniform distribution of the current density in a solid conductor surrounded by a magnetic material. 2D FEA analysis (top) and 3D FEA analysis (bottom).

This same leakage flux effect is usefully exploited in double cage asynchronous machine to enhance the starting torque.

The resistance ratio, K_{leak}, related to the slot leakage flux in a solid conductor surrounded by a magnetic material could be estimated as follows [6]:

$$K_{leak} = \frac{R_{AC}}{R_{DC}} = \xi \frac{\sinh(2\xi) + \sin(2\xi)}{\cosh(2\xi) - \cos(2\xi)} \tag{19}$$

where ξ is the reduced height of the conductor, and is expressed by:

$$\xi = h_{bar}\sqrt{\sigma\mu\pi f \frac{w_{bar}}{w_{slot}}} = \frac{h_{bar}}{\delta}\sqrt{\frac{w_{bar}}{w_{slot}}} \tag{20}$$

It must be pointed out that the relation 18 is valid for simple layer winding (one bar per slot), which corresponds to the winding we are proposing here. Otherwise, a second term must be added in the relation 18 to take into account the proximity effect between the different elementary layers.

4.2.2 The critic height of the bar, important notion

For a given width and frequency, a solid conductor surrounded by a magnetic material has an optimum height called *critic height*, h_{critic} [1, 6]. Indeed, h_{critic} is the threshold corresponding to the lowest AC resistance, under which the losses increase strongly, whereas if it is exceeded the losses tend to stagnate or increase very slightly in spite of the increase of the conductor cross-section. In other words, the critic height corresponds to the useful cross-section in which the current flows, so, it is useless to go beyond this critical height, however, if $h_{bar} < h_{critic}$ the losses will increase because the current density increases in the conductor.

For the sake of illustrating what has been said above, we performed a 2D finite element calculation of the AC Joule loss in a copper bar with: fixed width of 4 mm, variable height between 1 mm and 20mm, a length of 1 m, carrying an alternating current of 285 A_{rms}, and with parameterized frequency between 50 Hz and 1000 Hz. The results are presented on the **Figure 9**; we notice that there is an optimal height where the additional losses are minimal (minimum AC resistance) and which decreases with the frequency.

The h_{critic} can be defined by the following relationship [6]:

$$h_{critic} = \frac{1.32}{2\pi\sqrt{\frac{w_{bar}}{w_{slot}}\frac{f}{\rho 10^7}}} = 1.32\sqrt{\frac{w_{slot}}{w_{bar}}}\delta \tag{21}$$

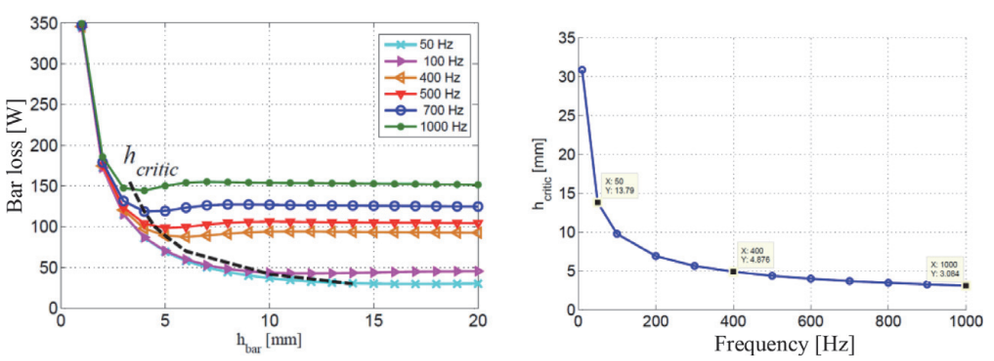

Figure 9.
AC copper loss at 20°C in a rectangular solid bar with wbar = 4mm– Illustration of the critic height of the bar: Finite element analysis (left) and analytical relationship (21) (right).

Where δ is the skin depth of the bar, $\delta = 1/\sqrt{\sigma\mu\pi f}$.

The h_{critic} calculated by the relationship (21), for the same bar width w_{bar} = 4 mm, is presented in the **Figure 9(b)**, it can be shown that the analytical calculation is in good general agreement with the finite element analysis in the **Figure 9(a)**.

As a rule of thumb, at 1 kHz operating frequency, at copper operating temperature around 150°C, the optimum copper bar height is around 4 mm.

4.2.3 Optimization of the AC loss in a solid conductor located in a magnetic core

To overcome the phenomenon of the uneven distribution of the current density due to the slot leakage flux, the most famous technique consists in subdividing the stator bars into parallel layers insulated from each other and regularly transposed along the length, so that each elementary conductor occupies different positions in the slot from the root to the head of the slot. With this technique the slot root inductance and the slot head inductance are balanced and the current tends to flow over the entire copper cross-sectional area. Consequently, the extra loss is tremendously mitigated and getting closer to the ohmic loss (DC loss). This technique is complex and impairs the copper fill factor compared to undivided bar due to the multiple insulations between the elementary conductors. It is commonly used for large generators (> 100MW rating) and called "*Roebel bar*".

Using insulated conductors with simple paralleling (without twisting) is not sufficient to reduce losses, because the bars create circulating currents between each other, resulting in additional losses identical to those produced in an equivalent solid bar. The 2D finite element simulation in **Figure 10** shows that the current density distribution in the parallel insulated conductors is the same with respect to a one solid bar (concentration near the slot opening).

However, the subdivision of the bar into *n* sub-conductors in series can optimize the AC copper losses by imposing a current of *I/n* in each elementary conductor independently of its position in the slot. However, it should be emphasized that this is subject to the judicious choice of the number of sub-conductor, otherwise, the additional loss can be significantly increased following an inadequate series connection (reverse effect).

4.3 Effect of the rotating field

In lesser extent, there is a third effect caused by the rotor field traveling in front of the stator which is represented by B_{mag} in **Figure 6**. In this case, it is the rotating

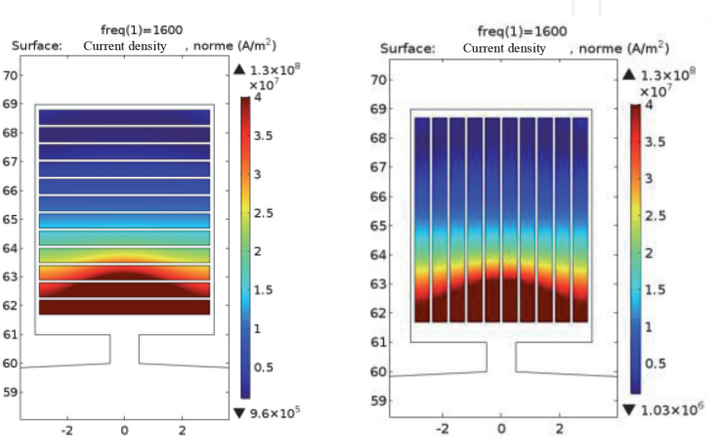

Figure 10.
Current density distribution in a copper bar following a simple paralleling.

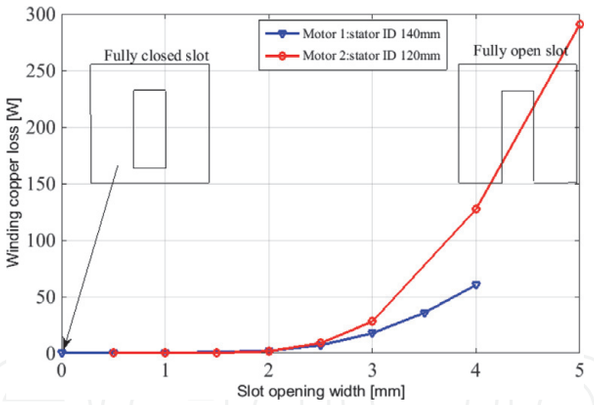

Figure 11.
Eddy-current loss in a solid bar due to the rotating field.

magnetic field of the permanent magnet mounted on the surface of the rotor. The variable B_{mag} could be seen by the solid conductors and, consequently, creates an extra eddy-current loss [1]. This loss component mainly depends on the slot opening and the saturation level of the iron surrounding the bar. If the slot is close enough the flux will be canalized by the iron and does not cross the copper. The typical slot opening width of the solid bar winding that we propose in this paper is between 0.5 and 1 mm (bar slipped into the slot). A finite element analysis, carried out on two different PM motors, has proven that the induced loss due to the rotating field is negligible for the slot opening lower than 2 mm, the results are shown in **Figure 11**.

5. Case study: FEA analysis, prototype manufacturing and testing

Many motor using the solid bar winding developed here were manufactured and tested successfully; all these motors were dedicated to the electric propulsion (e-Cars, e-Boats, ...).

The main characteristics of one of these motor are presented in the **Table 2**. The stator and rotor photos are presented in the **Figure 12**.

The first test was carried out at no load by driving the motor with another machine. The line to line back EMF was measured and showed a good agreement with the predicted back EMF via the commercial FEA tool ANSYS Maxwell (cf. **Figure 13**).

The electrical power at the input of the inverter driving the motor at no load was measured as well, this measurement represents the total no load losses of the motor. At 3700 rpm, the total no load losses are equal to 300 W, cf. **Table 3**.

Afterwards, a test rig was set up in back-to-back configuration (two identical motors) for the full load testing, as shown in **Figure 14**. The electrical power was measured at the output of the inverter driving one of the two motors by consuming the electrical power from the battery rack. The winding of the second motor is generating the power to charge the same battery. The output mechanical power was measured via a torque meter installed between the two motors.

The flux density and the full load torque were checked with ANSYS Maxwell and presented in the **Figures 15** and **16** respectively.

The extra on load losses dissipated in the motor were isolated based on the measurements and the AC copper losses predicted by means of the FEA analysis; the calculation is detailed in the **Table 3**. These extra losses present 8% of the total on load losses (42 W/520 W), they occur in any inverter fed electric motors and can be split into many components:

Dimensions	
Stator outer diameter	180 mm
Stator inner diameter	140 mm
Magnetic airgap	1,5 mm
Magent height	6.1 mm
Stator stack length	50 mm
Winding bar dimensions (hxw)	6x4 mm
Slot dimensions (hxw)	7x5 mm
Materials	
Stator corepack	M270-35A
Magnets	N35UH
Electrical parameters	
Pole number	16
Slot number	48
Phase resistance, 20°C - 100°C	1,3 mΩ - 1,7 mΩ
Phase inductance	12 µH
Back EMF coefficient ke	41,1 mVs/rd
Torque coefficient kt	0,123 Nm/A
Total weight (including mechanics)	10 kg
Nominal torque-to-weight ratio	2.5 Nm/kg
Cooling	Natural convection

Table 2.
Motor characteristics.

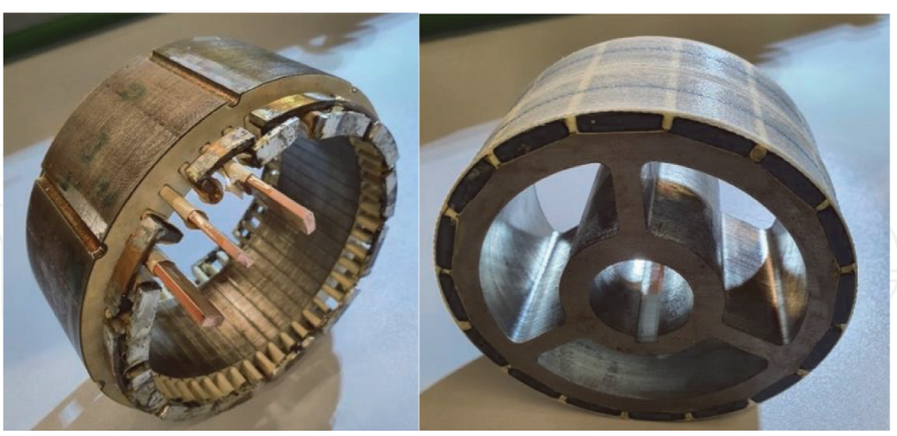

Figure 12.
Photo of the prototype. Left: Standalone wound stator with bar winding - Right: Glued magnets on the rotor wheel and sleeved rotor.

- The additional core loss due to the polluted current injected by the inverter.
- The extra AC copper loss due to the distorted current from the inverter (switching harmonics).
- Stray losses: these regroup all the "non-conventional" losses such as the eddy-current losses in the metallic structure of the motor (e.g. the end-windings leakage flux can generate eddy-currents in the flanges ...).

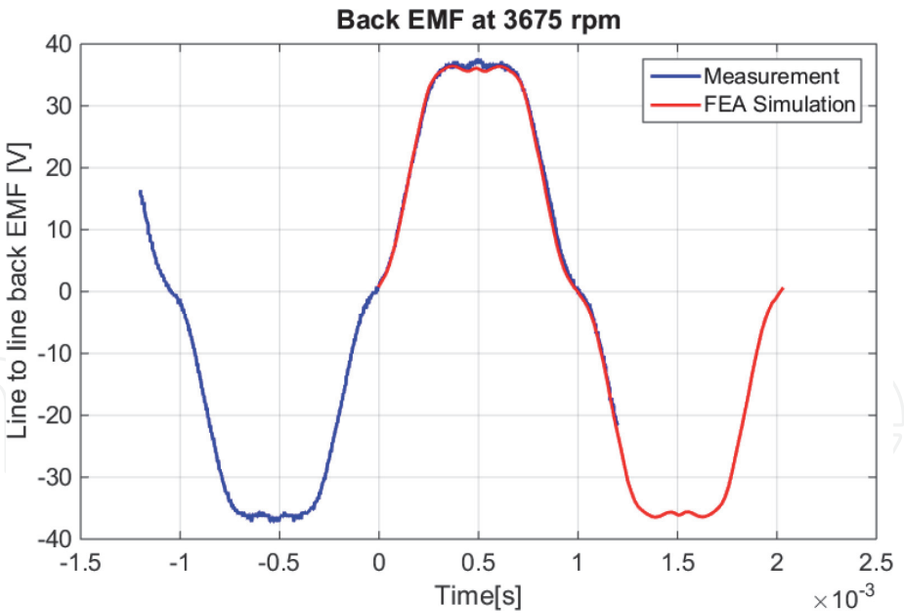

Figure 13.
Line to line back EMF at 3700 rpm and at 80°C magnet temperature.

(1)	Phase current [Arms]	170
(2)	Copper temperature [°C]	100
(3)	Speed [rpm]	3700
(4)	Frequency [Hz]	493.33
(5)	Torque [Nm]	20
(6)	Total phase resistance - Measured [mOhms]	1.7
(7)	Total phase resistance - copper in slots only [mOhms]	0.739
(8)	Total phase resistance - copper the end-windings only [(6)–(7)] [mOhms]	0.961
(9)	DC copper loss at end-windings only [W]	83.36
(10)	DC copper loss in the slots only [W]	64.03
(11)	Kleak relationship 18 in Section 4.2.1	1.59
(12)	AC copper loss in the slots only - Analytical prediction [(11) x (9)] [W]	101.81
(13)	AC copper loss in the slots only - 2D FEA Ansys Maxwell [W]	93
(14)	Total no load losses - Measured (no load core loss + mechanical losses) [W]	300
(15)	Magnet eddy-current loss - 2D FEA Ansys Maxwell [W]	1.4
(16)	Sleeve eddy-current loss (non conductive) [W]	0
(17)	Motor electrical input power - Measured [W]	8270
(18)	Motor mechanical output power - Measured [W]	7750
(19)	Motor total on load losses - Measured [(17)–(18)] [W]	520.00
(20)	Total additional losses [(19)–(15) - (14) - (13) - (9)] [W]	42.24
(21)	Efficiency of the motor - Measured [%]	93.712

Table 3.
Motor losses breakdown.

The different tests carried out have shown that the motor is able to reaches the required performance point of view output power, efficiency and thermal behavior. The total losses were proven to be at the predicted level.

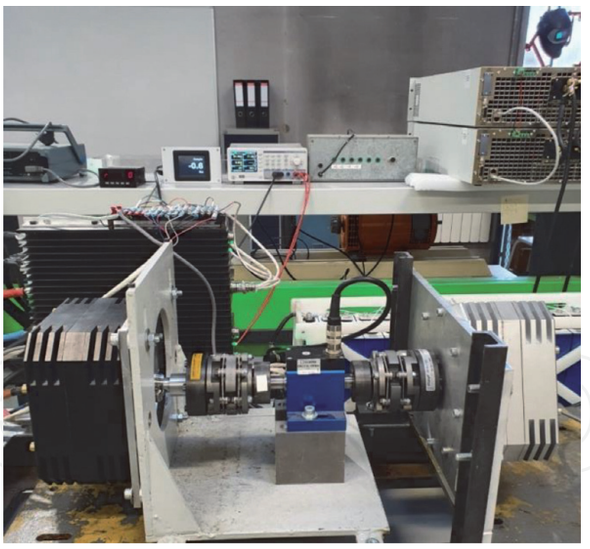

Figure 14.
Photo of the test rig – The identical motors are connected in back-to-back configuration.

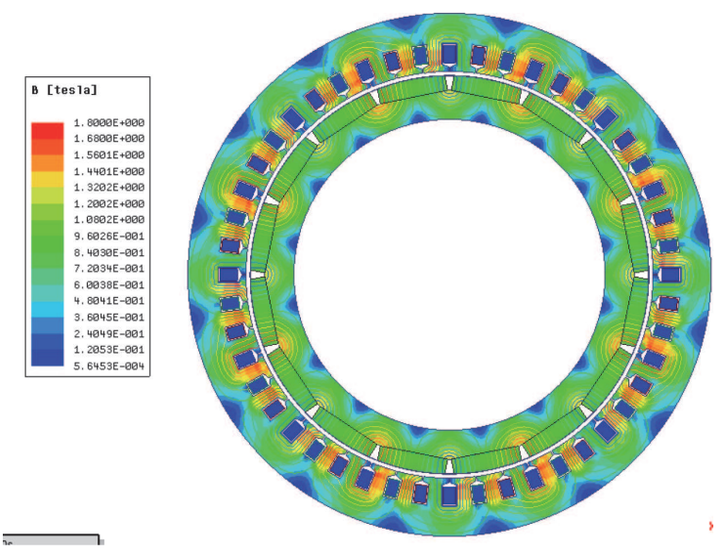

Figure 15.
On load flux density obtained from FEA analysis (ANSYS Maxwell) at 170 arms/20 nm.

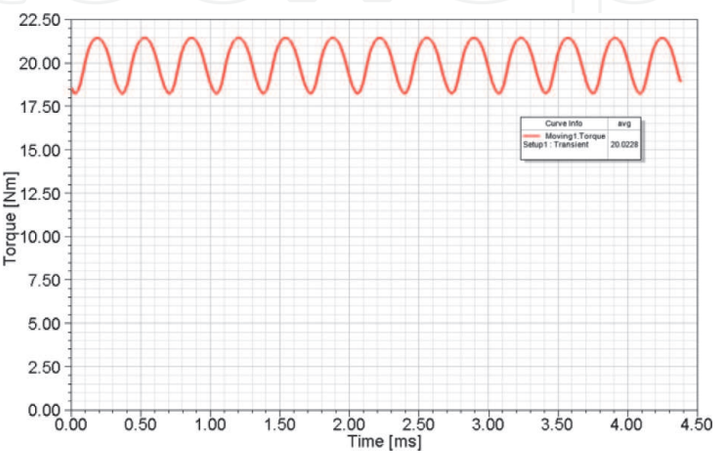

Figure 16.
Electromagnetic torque calculated by FEA at 170 Arms and 80°C magnet temperature.

Author details

Daniel Matt[1*] and Nadhem Boubaker[2]

1 University of Montpellier, Montpellier, France

2 Safran Electrical and Power, Pitstone, UK

*Address all correspondence to: daniel.matt@umontpellier.fr

IntechOpen

References

[1] Boubaker N. Study of atypical losses in high performance permanent-magnet synchronous machines for aircraft applications [thesis]. University of Montpellier; 2016.

[2] Enrici Ph, Boubaker N, Matt D. Bar Winding for the Low-Voltage Motorization of an Electric Tractor. In: Proceedings of the International Conference on Electrical Machines (ICEM); 23–26 August 2020; Gothenburg. Sweden: IEEE; 2005. p. 1711–1717

[3] Lorenzo P, Matt D, Gimeno A, Boubaker N. Contribution on AC bar windings losses reduction for a high frequency and high performance machine for aeronautical application. In: Proceedings of the International Symposium on Electromagnetic Fields in Mechatronics, Electrical and Electronic Engineering (ISEF); 29–31 August 2019; Nancy. France: IEEE; 2020. DOI 10.1109/ISEF45929.2019.9097026

[4] Boubaker N, Matt D, Enrici Ph, Nierlich F, Durand G. Measurements of Iron Loss in PMSM Stator Cores Based on CoFe and SiFe Lamination Sheets and Stemmed From Different Manufacturing Processes. IEEE Transactions on Magnetics. 2018; DOI: 10.1109/TMAG.2018.2877995

[5] Levasseur A. Nouvelles formules, valables à toutes les fréquences, pour le calcul. Journal de Physique et le Radium. 1930.

[6] Liwschitz M. Calcul des machines électriques. SPES; 1967. 276 p.